**Colloid & Polymer Science** Colloid Polym Sci 271:396–403 (1993)

# On the structure formation of hydrophobed particles in the boundary layer of water and octane phases

Z. Hórvölgyi*), G. Medveczky and M. Zrínyi

Department of Physical Chemistry, Technical University of Budapest, Hungary

*Abstract*: Two-dimensional aggregation of the surface modified glass beads was carried out in the boundary layer of water and octane phases. The effect of particles' hydrophobicity was investigated on the structure of forming aggregates and the growth process. The structure of the aggregates and their growth were characterized by a density function which demonstrates the change of mean particle density as a function of aggregate size. The growth yielded fractal or nonfractal structures in the investigated systems. The fractal structure of the aggregates was observed to be dependent on restructuring processes controlled by the surface properties of the beads.

The experimental results are compared with earlier findings for aggregation of hydrophobic beads in the boundary layer of water and air phases.

*Key words*: Hydrophobicity – contact angle – hydrophobic interaction – structure formation – fractal dimension – restructuring

## Introduction

The aggregation of fine, solid particles in the boundary layer of fluid/fluid phases is of great importance in many fields of natural and technological processes (scum formation on natural water, froth flotation, production of stable emulsions, etc.). On the other hand, the study of two-dimensional aggregation may also result in useful information for the three-dimensional aggregation phenomena.

Although, intensive investigations have been carried out on the characterization of aggregate structures [1–5], significant advances could be only reached in the past decade, due to the concept of fractal geometry of nature [6]. Both computer simulations as well as experimental works showed that the structure of aggregates formed under non-equilibrium conditions could be well characterized by the fractal dimension [7–11]. This is a structure parameter which makes possible to study the influence of several system parameters on aggregate geometry.

The aim of this work is to study the effect of hydrophobicity of colliding primary particles on growth phenomenon occurring in the boundary layer of water and octane phases, and on resultant aggregate structures. Earlier, the connection of hydrophobicity with such aggregate structures that formed in the boundary layer of water and air phases was studied [12]. It was emphasized that the role of restructuring, controlled by interparticle interactions, was of crucial importance in structure formation. In this work, we would like to demonstrate the common features of these phenomena, taking into account the colloid and capillary interactions between the beads.

## Experimental

### *Materials*

For the silylation procedure we used: *N,N*-dimethyl-trimethyl-silyl-carbaminate (gas chromatography purified [13]); *n*-hexane pure (Reanal) as the solvent; acetone A.R. (Reanal) as a washing

*) On leave from Loránd Eötvös University, Budapest, Hungary

liquid; mixture of cc. $H_2SO_4$ A.R. (Reanal) and 30 wt% $H_2O_2$ A.R. (Reanal) in 2 : 1 volume ratio, as a pretreatment agent of the glass surfaces.

For the aggregation experiments: glass beads with radius of 31–37 $\mu$m (Pyrex); microscope slides; double distilled water; *n*-octane pure (Ferak).

*Methods*

In order to study the connection of primary particles' hydrophobicity with the aggregate structures, two-dimensional aggregation of surface modified glass beads was carried out in the boundary layer of water and octane phases, at room temperature.

**The aggregation experiments** were accomplished in Petri dishes, with diameter of 11.5 cm. At first, the hydrophobed beads were dispersed in the octane phase, having a volume of 5–8 ml. Then, they were quickly poured onto the water in a Petri dish. The beads settled very rapidly into the boundary layer and were trapped there due to the capillary forces. This procedure resulted in individual beads at the beginning of aggregation experiments. As a consequence of temperature inhomogeneity, they began to move and collide. Their aggregation is attributed to capillary and colloid forces [12].

During the investigation, Petri dishes were covered by glass sheets in order to avoid the evaporation of octane and the pollution from the environment.

For structure analysis, nonequilibrium, different sized aggregates were photographed during the growth (20–20 pieces, respectively). The number of primary particles which formed an aggregate was in the range of 15–4000 in the case of the studied systems. The bead concentration was in the range of 30–40 pieces/cm$^2$ in the boundary layer at the beginning of aggregation. It should be noted that the complete aggregation took place in 1 h, and usually yielded one large aggregate.

**The aggregate structures** were characterized by using such density functions [12] which demonstrated the mean particle density ($\rho$) changing with the aggregates' characteristic size ($r$) in a log–log plotting, and by fractal dimension ($D$) determined from the linear part of the previous functions. In the case of fractal aggregates:

$$\rho \sim r^{D-d}, \tag{1}$$

where $d$ is the Euclidean dimension (In the case of fractal aggregates its value is always greater than $D$). The values of $r$ and $\rho$ were determined from the magnified image of aggregates. They were calculated by geometric mean method [14, 15] and from the ratio of primary particle number ($N$) and the aggregate area ($A$), respectively:

$$\rho = \frac{N}{A}. \tag{2}$$

The area of aggregate was approximated by $r^2$. "$r$" was accepted as $(xy)^{1/2}$ where "$x$" and "$y$" are the side-lengths of such rectangle which can be drawn around the aggregate and of which the longer side's length is equal to the distance of two points of the aggregate that are at the farthest separation.

For comparison, $D$ was determined with the aid of individual, great aggregates from the following relation, too:

$$\ln n_i \sim D \ln R_i, \tag{3}$$

where $R_i$ is the radius of the $i$th circle of which the center is the weight center of the aggregate and which covers $n_i$ pieces of primary particle ($i = 1, 2, 3, \ldots 15$). The maximal value of $R$ can be equal to the radius of gyration of the aggregate calculated by computer (concentric circle method [15]). One can obtain $D$ from this relation by the previous way.

**The surface properties of the beads** have been modified by a silylation procedure [16]. Various silylation conditions (reaction time and reagent concentration) yielded various hydrophobicity of the beads. The bead hydrophobicity was characterized by a mean water contact angle ($\Theta_Y$) which was calculated from the measured advancing ($\Theta_A$) and receding ($\Theta_R$) water contact angles, on the basis of the Wolfram–Faust equation [17]:

$$\cos \Theta_Y = \frac{\cos \Theta_A + \cos \Theta_R}{2}. \tag{4}$$

Considering the several difficulties connected with determination of bead wettability and bead immersion depth, $\Theta_A$ and $\Theta_R$ were measured by drop build-up technique, goniometrically, with a Rame-Hart NRL-100 device on a microscope slide which was silylated together with the beads. The greater the value of $\Theta_Y$, the higher the hydrophobicity of the surface.

In order to calculate the capillary interaction energies between two floating beads and their immersion depth in the water phase, advancing

water/octane contact angles ($\Theta_{A(w/o)}$) which formed on the beads in the boundary layer were also approximated in the previous way (measured in the water phase).

## Results

The values of $\Theta_Y$ and $\Theta_{A(w/o)}$ for the samples can be seen in Table 1.

In Figs. 1 and 2 images of different sized aggregates of the lowest and the highest hydrophobic systems are shown, respectively. For the greater aggregates in Figs. 1 and 2, fractal dimension ($D$), primary particle number of aggregate ($N$), and the radius of gyration ($R_g$) are presented in Table 2. They were determined by a computer.

In Fig. 3, 2–2 images of different aggregates of the highest hydrophobic system are shown to demonstrate different stadiums of the reorganization. In Fig. 4 the image of a large aggregate of the medium hydrophobic system can be seen.

On the basis of Figs. 1–4, it can be established that decreasing hydrophobicity yields looser aggregate structure. There is considerable difference in particle density between the lowest hydrophobic system and the other two. The values of particle densities for these two higher hydrophobic systems are rather close (Figs. 2 and 4).

It can be seen in Fig. 3 that reorganization of the aggregates leads to more compact structures during the growth. This type of restructuring, rotation of the bead segments, takes place in all systems, more or less. In the case of the lowest hydrophobic system, this type of reorganization is the most important secondary process. In the other two systems, another type of reorganization, characterized with side-by-side motion of the beads, is also significant, which leads to a more close-packed structure during growth. In these latter cases, bead segments are only observable for small aggregates (Fig. 3).

These visual observations are also supported by the density functions (Figs. 5–7). They resemble the density functions which were obtained for aggregates formed in the boundary layer of water/air phases [12]. It can be seen that aggregates' density for the lowest hydrophobic system decreases with aggregate size (i.e., during the growth) in the whole size range. For the other systems, above a critical aggregate size density increases with the size (shrinkage), which indicates the reorganization process characterized by the side-by-side motion of the beads. In accordance with former results [12], two different sloped lines may be fitted to the experimental points. The negative slope values indicate the fractal nature of aggregates. The critical aggregate size at which crossover (in the fractal property of the aggregates) occurs is in the range of 1.0–1.2 mm for the investigated systems. The

Table 1. The wettability parameters of the investigated systems

| $\Theta_{Y(water)}$ | $\Theta_{A(w/o)}$ |
|---|---|
| 73° | 110° |
| 81° | 123° |
| 88° | 136° |

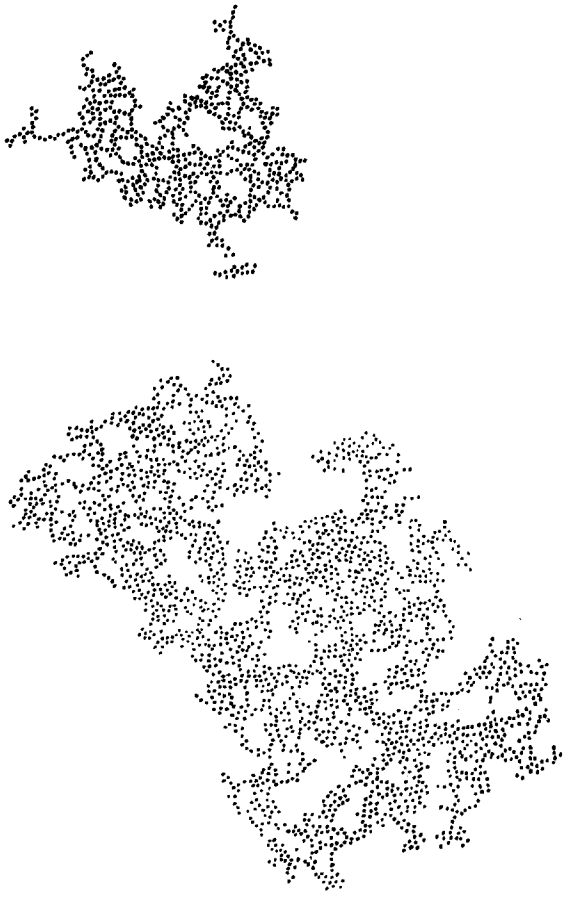

Fig. 1. A small and a large aggregate for the lowest hydrophobic system

Fig. 2. A small and a large aggregate for the highest hydrophobic system

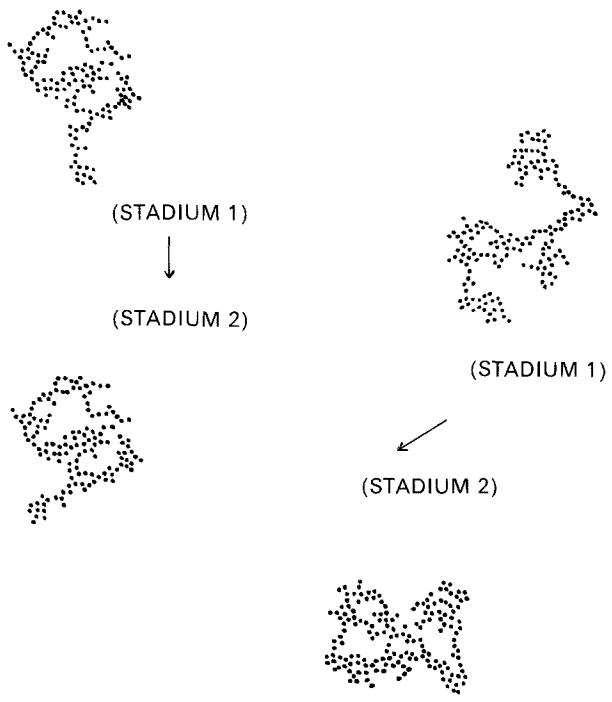


Fig. 3. Demonstration of restructuring for the highest hydrophobic system.

Table 2. The characteristic parameters of two individual, large aggregates of the lowest and the highest hydrophobic system ($R_g$ is the radius of gyration.)

| $\Theta_Y$ | 73° | 88° |
|---|---|---|
| $D$ | 1.8 | 2 (nonfractal) |
| $N$ | 2341 | 2001 |
| $R_g$ | 2.1 mm | 1.6 mm |

calculated fractal dimensions, the correlation coefficients, and the indication of density changing during the growth are given in Table 3. It can be seen that lower hydrophobicity of the primary particles yields lower fractal dimensions for the small aggregates. While in the case of the lowest hydrophobic system, fractal aggregates were also observed ($D = 1.84$) in the range of large aggregates, until the similar-sized aggregates of the other systems were found to be nonfractal. These findings are confirmed by the structure analysis carried out for individual, large aggregates of the lowest and the highest hydrophobic systems. They were found to be fractal and nonfractal, respectively (Table 2).

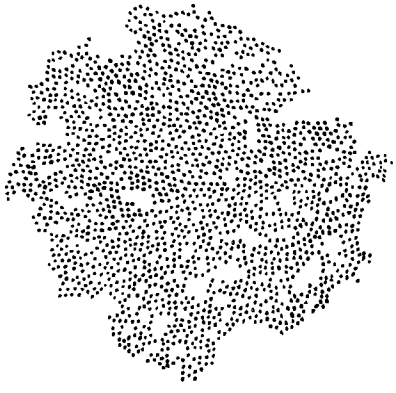

Fig. 4. A large aggregate for the medium hydrophobic system

## Discussion

According to former results of experimental works [18–22] and computer simulations [23–30], it is thought that the main reason for this behaviour of density functions and fractal dimensions is the restructuring controlled by interparticle interactions. In our previous work [12], it was found that

Table 3. The characteristic parameters of the investigated systems determined on the basis of density functions

| $\Theta_Y$ | $D$ (for small aggregates) | Changing in density with the aggregate size (for large aggregates) |
|---|---|---|
| 73° | 1.29( − 0.86) | decrease ($D$ = 1.84) |
| 81° | 1.26( − 0.80) | increase (shrinkage) |
| 88° | 1.71( − 0.46) | increase (shrinkage) |

Standard deviation of $D$ values: ∓ 0.1. The correlation coefficients are given in the brackets

Table 4. The energy values of capillary interaction calculated between two beads for the investigated systems in the contact position. During the calculations as a mean bead radius, 34 μm was used

| $\Theta_{A(w/o)}$ | Energy of the capillary interaction (J) |
|---|---|
| 110° | $-7.3 \times 10^{-17}$ |
| 123° | $-7.3 \times 10^{-17}$ |
| 136° | $-7.7 \times 10^{-17}$ |

increasing hydrophobicity of the beads yielded looser and more stringy (characterized by lower value of $D$) aggregates, because, the higher hydrophobicity resulted in stronger attractive (hydrophobic) interparticle interactions [31] by means of reorganization after the "primary growth" was slightly hindered. In this work, a reverse dependence was found between the hydrophobicity and the structure parameters ($D$, $\rho(r)$). In order to understand this apparent contradiction, a short analysis of interparticle interactions in the actual systems is made.

### *Connection of hydrophobicity with the interparticle interactions*

The hydrophobicity influences the capillary interaction between the beads (Appendix 1). The calculated value of capillary interaction energies for the contact position of two floating beads is shown in Table 4.

It can be seen that there is no relevant difference between the systems. It should be noted that the changing of these values, below the bead distance of 10 μm, is only of a few percent. On the basis of this result, it seems that the capillary interaction cannot be responsible for differences found in structure formation of the investigated systems.

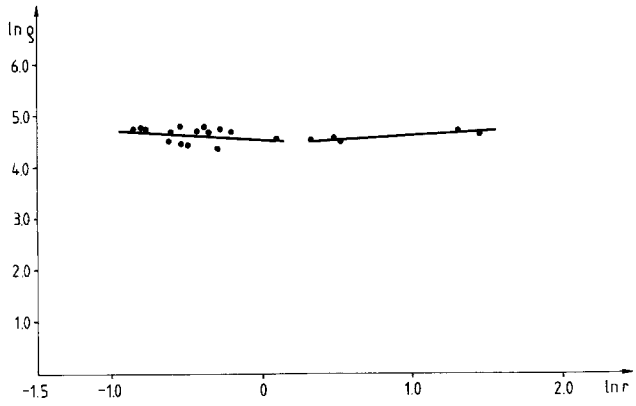


Fig. 5. Density function for the beads having the highest hydrophobicity ($\Theta_Y$ = 88° and $\Theta_{A(w/o)}$ = 136°)

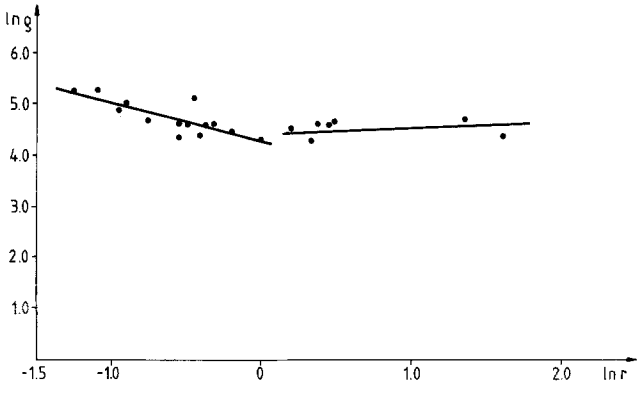


Fig. 6. Density function for the beads having medium hydrophobicity ($\Theta_Y$ = 81° and $\Theta_{A(w/o)}$ = 123°)

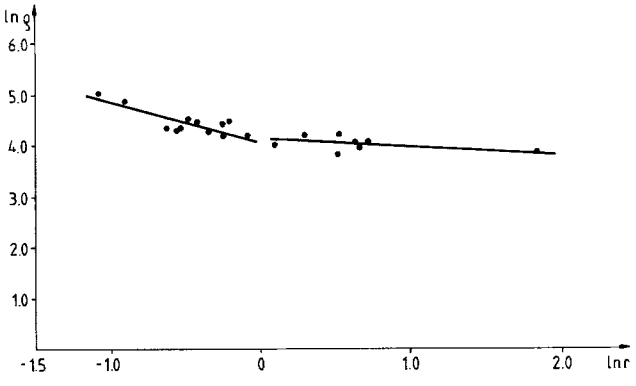


Fig. 7. Density function for the beads having the lowest hydrophobicity ($\Theta_Y$ = 73° and $\Theta_{A(w/o)}$ = 110°)

However, the hydrophobicity also influences the immersion depth of the beads (see Appendix 2). The calculated immersion depths are given in Table 5. It can be seen that the lower the hydrophobicity of the beads, the greater the immersion depth in water phase. Thus, a considerable part of the lowest hydrophobic beads can be immersed in the water. It is well known that the particles' situation in the boundary layer of two phases influences the colloid interaction between them [32, 33]. In Table 6, the most important types of bead interactions are shown acting in the water and oil phases.

In Table 7, the smallest, calculated values of bead–bead distances via the water phase are given (see Appendix 3). The calculated results show important differences between the systems. Nevertheless, these differences cannot be responsible for different structure formation of the investigated systems, because at these interparticle distances the colloid interactions are rather weak. On the other hand, the resultant aggregate structures (or rather, their density function and fractal dimension) of the lowest hydrophobic system, resemble those formed in the boundary layer of water and air phases as a result of the aggregation of the highest hydrophobic glass beads [12]. This system was established to be under the control of very strong hydrophobic interaction. As it was mentioned in the experimental part of this paper, our contact angle measurements were carried out on microscope slides which were surface-treated together with Pyrex glass beads. There are two important consequences of this procedure. First, the sylilation after an acidic pretreatment leads to more hydrophobic surface for glass having higher alkali content [35]. While Pyrex glass contains 4–6% $Na_2O$, the $Na_2O$–$K_2O$ content of an ordinary (microscope slide) glass is higher than 10%. As a consequence of this, slight differences can be seen between these surfaces in hydrophobicity characterized by the mean contact angle ($\Theta_Y$) and/or advancing contact angle.

Secondly, the two-liquid contact angle measurements usually more sensitively indicate differences between the solid surfaces than the one-liquid measurements [36]. Therefore, the contact angles measured on microscope slides can only indicate the tendency of hydrophobicity change for the bead samples. On the basis of these considerations, it is thought that the lowest hydrophobic beads are immersed more deeply in the water than the calculations showed. It is supposed that these beads may be close to a half-immersed situation. Considering the nonequilibrium feature of hydrophobic interaction and the results of Schulze [37], who emphasized the instability of even a considerably thick (170 nm) water film on very hydrophobic surfaces, it may be thought that the water interlayer between the lowest hydrophobic, colliding beads can break up, by means of which action the beads can reach the primary potential energy minimum where there will be strong, attractive interaction between them. For the other two systems, it is thought that beads can only be in the secondary minimum because significant hydrophobic interaction cannot act between them because of the greater bead–bead distances in water. (Secondary minima in these

Table 6. The most important colloid interparticle interactions which exist in water and oil phases

| Hydrophobed glass bead interactions in water phases | in octane |
|---|---|
| electrostatic double layer interaction (repulsive); dipole–dipole interaction (repulsive) [34]; dispersion interaction (attractive); hydrophobic interaction | solvation interaction (repulsive); dispersion interaction (attractive); |

Table 5. The calculated immersion depths in the water phase for the investigated systems

| $\Theta_{A(w/o)}$ | Immersion depth in $\mu$m | Immersion depth in bead radius ($a$) |
|---|---|---|
| 110° | 22.4 | 0.66 |
| 123° | 15.6 | 0.46 |
| 136° | 9.5 | 0.28 |

Table 7. The smallest bead–bead distances ($h$) via the water phase calculated for the smallest and for the greatest bead radii (31 and 37 $\mu$m)

| $\Theta_{A(w/o)}$ | $h$ in $\mu$m | $h$ in bead radius ($a$) |
|---|---|---|
| 110° | 3.7–4.4 | 0.12 |
| 123° | 9.9–11.8 | 0.32 |
| 136° | 18.9–22.6 | 0.61 |

cases are mainly attributed to the superposition of the very short-range, repulsive solvation [38] and the longer range, attractive dispersion forces.) Hence, they can move relatively easily side-by-side after the sticking which leads to shrinkage of their aggregates. This oversimplified analysis is also supported by the influence of dispersion forces, since the higher the hydrophobicity of the beads, the weaker the dispersion forces between them, because, via the octane phase (as a similar medium to the hydrophobed surfaces) weaker dispersion forces act than via the water phase.

It should be noted that fractal dimensions for the lower hydrophobic systems, of which values were found to be the same (1.26–1.29), are in accordance with that predicted by the tip-to-tip, cluster-cluster aggregation model [39–41]. This rather low value of fractal dimension is attributed to the anisotropic, repulsive, electrostatic interaction [39]. In our case, the beads of two lower hydrophobic systems can immerse deeply enough in the water, and considerable double layer and dipole–dipole electrostatic, repulsive forces can act between their aggregates, which can be responsible for lower values of fractal dimensions obtained. (In the meantime, the effect of ionic strength on the structure formation for this bead-size range at aqueous solution of electrolyte-air interfaces was proved experimentally [42]. Nevertheless, we think that the effect of repulsive electrostatic forces on the structure formation is not quite clear, and further intensive study is necessary for a better understanding of this complicated problem, taking into account some hydrodynamic and capillary effects.

## Appendix

1. The capillary interaction energy between two floating beads was calculated by the following relation of Chan et al. [43]:

$$V_c = \frac{2\pi a^6}{\gamma_{w/o}}(\rho_w - \rho_o)^2 g^2 S^2 \ln[\lambda(H + 2a)] \,. \quad (5)$$

This relationship is valid in the case of $\lambda(H + 2a) \ll 1$. $S$ is a parameter which involves the effect of hydrophobicity:

$$S = \frac{2}{3}\frac{\rho_s - \rho_o}{\rho_w - \rho_o} + \frac{1}{6}\cos\Theta^3_{A(w/o)} - \frac{1}{2}\cos\Theta_{A(w/o)} - \frac{1}{3} \,, \quad (6)$$

$\lambda$ is such a parameter of which reciprocal value ($\lambda^{-1}$) gives an approximation for the length at which water/octane interface is curved around a floating bead.

$$\lambda = \left(\frac{\rho_w - \rho_o}{\gamma_{w/o}}\right)^{1/2}. \quad (7)$$

According to this, two floating beads feel each other within a distance of some millimetres.

List of symbols:

$V_c$ – capillary interaction energy;
$a$ – bead radius;
$\gamma_{w/o}$ – interfacial tension of water and octane (assumed 50 mN/m);
$\rho_w$ – density of water (assumed $10^3$ kg/m$^3$);
$\rho_o$ – density of octane (assumed 703 kg/m$^3$);
$\rho_s$ – density of bead (assumed $2.45 \times 10^3$ kg/m$^3$);
$g$ – gravitational acceleration (9.8 m/s$^2$);
$H$ – distance between two beads;
$\Theta_{A(w/o)}$ – two-liquid advancing contact angle;

2. The calculation of the beads' immersion depths ($k$) was accomplished as follows (also see Fig. 8):

$$k = a[1 - \cos(180° - \Theta_{A(w/o)})] \,. \quad (8)$$

This relationship can be used if the gravitational effect is negligible [44]. This condition is valid for our small bead sizes [45], i.e., the two-liquid interface around the bead may be considered as flat from this aspect.

3. The calculation of the smallest bead–bead distance ($h$) via the water phase, for the contact

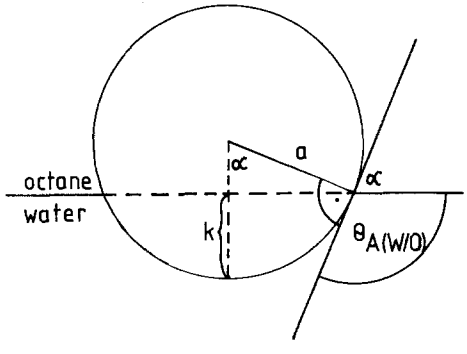


Fig. 8. Drawing of a bead in the boundary layer of water and octane phases and the parameters for the calculation of immersion depth

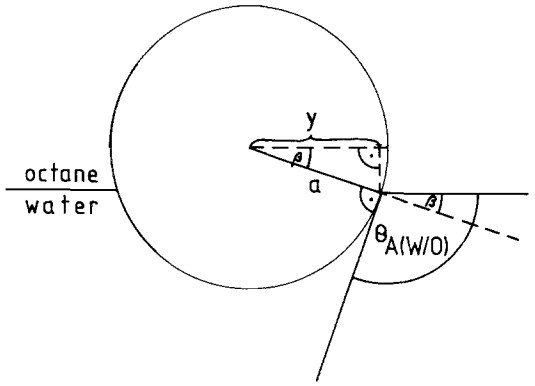


Fig. 9. Drawing of a bead in the boundary layer of water and octane phases and the parameters for the calculation of the smallest bead–bead distance ($h$) via the water phase ($2(a - y) = h$)

position, was carried out as follows (also see Fig. 9):

$$h = 2a[1 - \cos(\Theta_{A(w/o)} - 90\,^\circ)] \,. \qquad (9)$$

This relationship can also be used if the gravitational effect is negligible.

*Acknowledgements*

We gratefully acknowledge the help rendered by Professor H. G. Kilian and M. Bratrich, Ulm University. We thank Dr. Márta-Kabai Faix for the valuable discussion. This work was supported by the Hungarian Academy of Sciences (OTKA 2166-5-373).

**References**

1. Vold MJ (1963) J Colloid Sci 18:684
2. Sutherland DN (1966) J Colloid Interface Sci 22:300
3. Medalia AI (1967) J Colloid Interface Sci 24:393
4. Medalia AI (1970) J Colloid Interface Sci 32:115
5. Medalia AI, Heckman FA (1971) J Colloid Interface Sci 36:173
6. Mandelbrot BB (1982) The Fractal Geometry of Nature. Freeman WH and Company, New York
7. Herrmann HJ (1986) Physics Reports 136:153
8. Meakin P (1988) Advances Colloid Interface Sci 28:249
9. Vicsek T (1989) Fractal Growth Phenomena. World Scientific, Singapore, New Jersey, London, Hong Kong
10. Jullien R, Botet R (1987) Aggregation and Fractal Aggregates. World Scientific, Singapore
11. Allain C, Cloitre M (1986) Phys Rev B 33:3566
12. Hórvölgyi Z, Medveczky G, Zrinyi M (1991) Colloids Surfaces 60:79
13. Knausz D, Meszticzky A, Szakács L, Csákvári B, Ujszászy K (1983) J Organometal Chem 256:11
14. Samson RJ, Mulholland GW, Gentry JW (1987) Langmuir 3:272
15. Hórvölgyi Z, Kabai-Faix M, Zrínyi M (1990) In: Proc of 5th International Conf on Colloid Chem. Balatonfüred, Hungary (1988); Kiss É, Pintér J (eds), Loránd Eötvös University, Budapest, pp 338–341
16. Hórvölgyi Z, Kiss É, Pintér J (1986) Magy Kém Foly 92:486
17. Wolfram E, Faust R (1978) In: Padday JF (ed) Wetting Spreading and Adhesion. Acad Press, London, 213
18. Dimon P, Sinha SK, Weitz DA, Safinya CR, Smith GS, Varady WA, Lindsay HM (1986) Phys Rev Lett 57:595
19. Aubert C, Cannell DS (1986) Phys Rev Lett 56:738
20. Skjeltorp AT (1987) Phys Rev Lett 58:1444
21. Medveczky G (1990) M.Sc. Thesis, L Eötvös University, Budapest
22. Adachi Y, Ooi S (1990) J Colloid Interface Sci 135:374
23. Meakin P, Jullien R (1985) J Phys 46:1543
24. Botet R, Jullien R (1985) Phys Rev Lett 55:1943
25. Meakin P (1985) J Chem Phys 83:3645
26. Meakin P, Deutch J (1985) J Chem Phys 83:4086
27. Meakin P (1986) J Colloid Interface Sci 112:187
28. Kolb M (1986) J Phys A 19:L263
29. Kolb M (1986) Phys Rev Lett 56:2769
30. Jullien R, Meakin P (1989) J Colloid Interface Sci 127:265
31. Derjaguin BV, Churaev NV (1989) Colloids Surfaces 41:223
32. Levine S, Bowen BD, Partridge SJ (1988) Colloids Surfaces 38:325
33. Levine S, Bowen BD, Partridge SJ (1988) Colloids Surfaces 38:345
34. Pieranski P (1980) Phys Rev Lett 45:569
35. Bouquet G, private communication
36. Wolfram E (1971) In: Csákvári B (ed) A kémia újabb eredményei, Kontakt nedvesedés, Akadémiai Kiadó, Budapest, pp 7–130
37. Schulze HJ (1984) Developments in Mineral Processing. Elsevier, Amsterdam
38. Christenson HK, Horn RG, Israelachvili JN (1982) J Colloid Interface Sci 88:79
39. Hurd AJ, Schaefer DW (1985) Phys Rev Lett 54:1043
40. Jullien R (1985) Phys Rev Lett 55:1967
41. Jullien R (1986) J Phys A 19:2129
42. Hórvölgyi Z, Máté M, Zrínyi M (1992) 6th International Conf on Colloid Chem. Balatonszéplak, Hungary, Proceedings, Abstr. 70
43. Chan DYC, Henry JD Jr, White LR (1981) J Colloid Interface Sci 79:410
44. Princen HM (1969) In: Matijevic E (ed) Surface and Colloid Science Vol. 2. The Equilibrium Shape of Interfaces, Drops, and Bubbles. Rigid and Deformable Particles at Interfaces. Wiley Interscience, New York, London, Sydney, Toronto, pp 1–84
45. Tschaljovska SD, Aleksandrova LB (1978) Chem Techn 30:301

Received October 7, 1991;
accepted June 10, 1992

Authors' address:

Dr. Zoltán Hórvölgyi
Department of Physical Chemistry
Technical University of Budapest
Egry j.u. 20-22
H-1111 Budapest
Hungary